On the subwavelength structure of the evanescent field of an optical Bloch wave

R.J.P. Engelen[1], D. Mori[2], T. Baba[2], and L. Kuipers[1]
[1] *Center for Nanophotonics, FOM Institute for Atomic and Molecular Physics (AMOLF), Kruislaan 407, 1098 SJ Amsterdam, The Netherlands*
[2] *Yokohama National University, Department of Electrical and Computer Engineering, 79-5 Tokiwadai, Hodogayaku, Yokohama 240-8501, Japan*
(Dated: July 28, 2008)

We have measured the three-dimensional distribution of the evanescent field above a nanophotonic structure, a photonic crystal waveguide. The periodic structure of the photonic crystal causes the propagating waves to be governed by Bloch's theorem: they are composed of multiple wavevectors or harmonics. The Bloch character of the light has a profound influence on its evanescent field. We found, by measuring the field with phase-sensitive near-field microscopy, that the evanescent field of the composite Bloch wave decays non-exponentially as a function of height. Even the individual Bloch harmonics, having only a single wavevector, do not necessarily decay single-exponentially. This effect has its origin in the intricate in-plane field distribution of each harmonic. The complex decay leads to an evolution of the mode pattern as a function of the height above the structure. Our experimental results are confirmed with calculations.

PACS numbers: 42.70.Qs, 42.82.Et, 68.37.Uv

Sir Isaac Newton was the first to report on the evanescent field. He observed frustrated total internal reflection and concluded from his measurements that the evanescent field extends approximately "ten hundred thousandth Part of an Inch" (25 nm) [1]. The evanescent field is exploited for a broad range of applications, ranging from coupling of light in and out of structures [2] to two-dimensional Bose-Einstein condensation [3], strong coupling [4], sensing [5], subwavelength focusing [6] and microscopy [7].

The school book example of an evanescent wave is that of total internal reflection at a planar interface from a high dielectric constant (ϵ) to a low-ϵ material. Above the interface ($z > 0$) the field decays according to

$$E(z,t) = E(0,t)\mathrm{e}^{iz\sqrt{\epsilon_{low}\frac{\omega^2}{c^2}-k_\parallel^2}}, \qquad (1)$$

where the optical frequency is denoted as ω, c is the speed of light in vacuum. For evanescent waves, the exponent is real and negative resulting in an exponentially decaying field away from the interface. The above equation holds for flat planar interfaces but not only for total internal reflection but also for, amongst others, light propagating in thin slabs of material, or surface waves like surface plasmon polaritons. The evanescent field of periodically patterned surfaces may differ however.

An intriguing class of periodically structured optical materials are photonic crystals, in which materials with a high and a low ϵ are arranged in a lattice. The periodic structure greatly affects the propagating of light [8–11]. Light in a photonic crystal, must obey Bloch's theorem, which dictates that the amplitude of a wave must conform to the imposed periodicity [12]. The resulting wavefunction ψ, simplified to one dimension, can be described as

$$\psi(y) = u_k(y)\exp(iky), \text{ where } \; u_k(y) = u_k(y+a). \qquad (2)$$

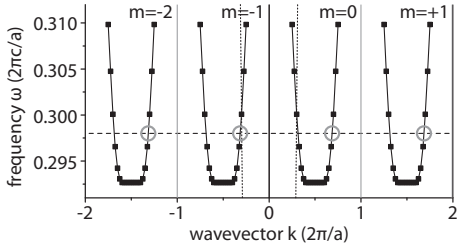

FIG. 1: Portion of the dispersion relation of the photonic crystal waveguide under investigation, obtained via 3D FDTD simulations (solid squares). The solid lines are guides to the eye. An excited Bloch mode at ω=0.298 has multiple wavevectors (encircled intersections), spaced ($2\pi/a$) apart. The vacuum mode (or light line, $\omega = ck$) is depicted with the dotted line.

The above equation, with wavevector k and a periodic amplitude modulation $u_k(y)$, with the same period (a) as the lattice, can be rewritten as a Fourier series of plane waves:

$$\psi(y) = \sum_m a_m \exp(i(k + m\frac{2\pi}{a})y), \text{ where } \; m \in \mathbb{Z}, \qquad (3)$$

which describes that the individual plane waves that together make up the Bloch wave, the harmonics, each have an amplitude a_m. Their wavevector is k plus an integer (m) number of the reciprocal lattice period $2\pi/a$. Based on Eq. 2, one might naively expect an exponential decay for the evanescent field, governed by the magnitude of $k_\parallel$ ($= k$) (see Eq. 1). The multiple harmonics in Eq. 3 however suggest that the decay is multi-exponential [13].

In this Letter, we have investigated the evanescent field above a two-dimensional photonic crystal waveguide with three-dimensional near-field microscopy. We will show both with experiments and calculations that both the Bloch nature of the guided light but also the confinement

of light in a narrow waveguide, has a profound effect on the evanescent field above the structure. We find a highly complex decay behavior. As a result, also the field patterns above the structure strongly evolve with height.

The photonic crystal structure we investigated, is a 200-nm thick air-bridge membrane of Si. In the membrane, we etched a hexagonal lattice (period $a = 456$ nm) of air holes (radius 140 nm). A single row of holes is not perforated and acts as a waveguide. At each side of the waveguide, 10 rows of holes provide ample confinement of the light by the photonic bandgap [14]. At the outermost row of holes, the energy of the field is reduced by 6 orders of magnitude. The transmission loss due to fabrication disorder is estimated to be a few dB/mm, which constitutes a negligible loss at the length scales relevant for the work presented here (< 100 μm). Figure 1 shows a portion of the calculated dispersion relation of the waveguide under investigation. The encircled intersections indicate the wavevectors, each spaced $2\pi/a$ apart, that together form the Bloch wave, that are excited at a specific optical frequency (ω=0.298, dotted line). Note that the non-encircled set of intersections corresponds to the backward propagating wave.

We measured the optical field above the structure with a phase-sensitive near-field microscope [15]. By scanning a metal-coated tapered optical fiber over the structure, we obtain a map of the optical field above the structure. By incorporating the scanning setup in a heterodyne interferometer, we recover the electric (E-)field amplitude and phase locally. The diameter of the probe aperture is 200 nm determines, on first approximation, the detection area of $3.1 \cdot 10^{-14}$ m^2. The collected power by the probe is expressed as a power density in units W/m^2. Figure 2a shows the power density of the field, at ω=0.298 where the distance of the probe to the sample is kept constant at 10 nm. The measurement clearly shows that the light is confined to the waveguide, centered along the line $x = 2.6$ μm.

By Fourier transforming the measured complex field along the direction of the waveguide (y-direction), we retrieve the periodic components of the field: the wavevectors k_y [16]. Figure 2b shows the power spectrum obtained by summing the square of the amplitude of the Fourier transforms for all x values. In agreement with the dispersion relation shown in Fig. 1, we find peaks at $k_y = 0.68 \pm m$ in normalized units of $2\pi/a$, with m being an integer. The asterisks in Fig. 2b indicate the wavevectors of the wave reflected at the end facet of the waveguide.

In order to recover the spatial distribution of each Bloch harmonic, we applied a Fourier filter to the complex field data underlying Fig. 2a. Figure 2c shows the Fourier filtered data, with a Gaussian selection window centered around $k_y = 0.68$ and with a width of 0.02 (see Fig. 2b). We define the harmonic with $k_y = 0.68$ as the fundamental Bloch harmonic with $m = 0$. The same filter is applied for the $m = -1$ harmonic ($k_y = -0.32$), of which the results are depicted in Fig. 2d. For the fundamental wavevector we find a similar distribution as in 2a: the power density is highest in the center of the image, around $x = 2.6$ μm. The power density distribution of the $m = -1$ harmonic is however more extended into the crystal region. We attribute this difference to the intricate modal pattern of the composite Bloch wave, which exhibits stronger amplitude variations towards the crystal region, requiring the harmonics $m \neq 0$ to be stronger.

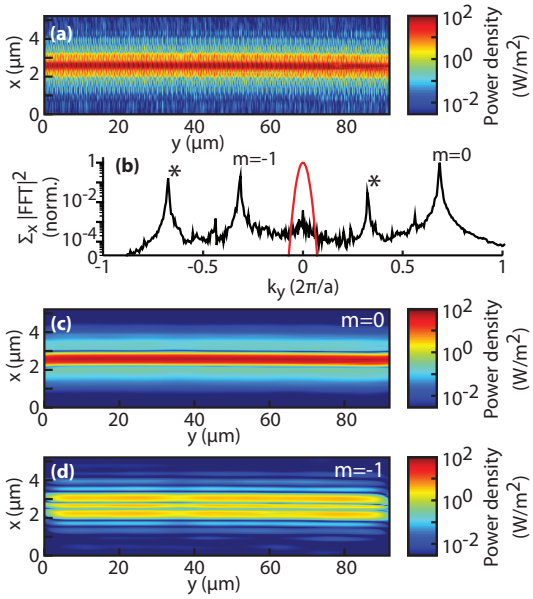

FIG. 2: (a) Colorscale (logarithmic) image of the measured power density distribution. The waveguide is centered along the $x = 2.6$ μm line. (b) Power spectrum of the k_y wavevectors present in the structure, obtained via Fourier transforming the complex phase-sensitive E-field distribution underlying (a). Two Bloch harmonics are visible ($m = -1$ and $m = 0$) and two wavevectors of the reflected Bloch wave ($*$). The red line depicts the window of the Fourier filter (not necessarily at $k_y = 0$), used to extract the power density distribution of the fundamental and $m = -1$ harmonic, respectively (c,d), obtained via Fourier filtering the complex phase-sensitive E-field distribution underlying (a).

To determine the decay of the evanescent field above the photonic crystal waveguide, we performed a series of measurements, each with a different distance of the probe to the sample z. Using the same Fourier filtering procedure as describe above, we calculated the power density for each height. We used appropriate Fourier filtering (see above), to recover the power density for the harmonics with $m = -2,\ -1,\ 0$ and $+1$. Each of these harmonics can have a different lateral power distribution (the amplitudes a_m in Eq. 3 are allowed to depend on x). We therefore integrated over the distribution perpendicular to the waveguide, to obtain the power per unit length of waveguide. The result is depicted in Fig. 3, showing the power as a function of height.

Perhaps surprisingly, the curves show that each harmonic decays with a different slope as the height increases, until the curves level off at a power per unit

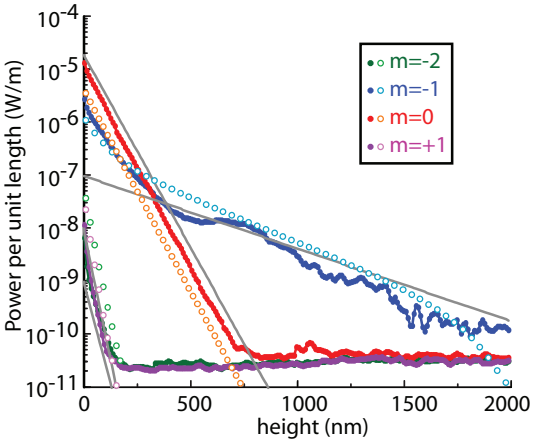

FIG. 3: Measured power in each of the Bloch harmonics as a function of probe-sample height z for four harmonics (see legend). Both the measurement results (solid dots) and the 3D FDTD results (circles) are shown. The grey lines indicate the decay expected based on Eq. 1 and are offset for clarity.

length of $\sim 3 \cdot 10^{-11}$ W/m, where the noise level of the analysis is reached. The harmonics with the largest wavevectors ($m = -2$ and $m = +1$), have the strongest decay ($k_z \approx 20i\ \mu\text{m}^{-1}$), whereas the harmonic with the smallest wavevector ($m = -1$), decays very slowly as a function of height ($k_z \approx 2i\ \mu\text{m}^{-1}$). The ensemble of these harmonics together form the Bloch wave, while the individual harmonics are not a solution to Maxwell's equations. Adding the harmonics of Fig. 3 yields a decay that is dominated by the fundamental harmonic close to the surface ($z < 250$ nm), but at larger distances ($z > 500$ nm), the $m = -1$ harmonic dominates. Obviously, the Bloch wave itself, which is composed of these harmonics, therefore does not exhibit a single exponential decay.

The differences in decay can be understood by considering Eq. 1, since each harmonic has a different wavevector $k_\parallel$, the decay must consequently also differ. Since the parallel wavevectors of the $m = -2$ and $m = +1$ harmonic are much larger than the low-ϵ wavevector (air), their decay is rapid. The $m = -1$ harmonic on the contrary, which has a wavevector very close to the vacuum wavevector, decays much more slowly. The decays expected based on Eq. 1 are depicted with the solid lines, but they do not fully describe the measured decays. In particular, a strong deviation is found for the $m = -1$ harmonic: between 0 and 400 nm: the experimentally found decay is much stronger than a single exponential decay expected based on Eq. 1.

We have performed 3D finite-difference time-domain (FDTD) simulations [17] to validate our experimental results and to confirm the deviation from a single-exponential decay. We applied a similar Fourier analysis to the FDTD data to resolve the individual Bloch harmonics. The results are also depicted in Fig. 3. We concluded from the comparison of the results that there is qualitative agreement between FDTD results and experiment. There are some differences in relative amplitude between the harmonics, which we attribute to the wavevector dependent coupling to the near-field probe [18].

Key to the full understanding of the complex decay of the Bloch harmonics and the composite Bloch wave are the lateral modal profiles (perpendicular to the waveguide direction) as a function of height. We have plotted the experimental and simulated results for the fundamental harmonic in Figs. 4a and 4b, respectively, which clearly are in good agreement. Note that the backward propagating harmonics (asterisks in Fig. 2b) show the same behavior. The evanescent field has nodes (arrows in Fig. 4b), with fields with opposite signs on either side, as is indicated by '+' and '-'. On close examination, one can observe that the field profile broadens as the height is increased: the nodes in Figs. 4a and 4b shift outward as the mode pattern changes as a function of height. This is quite in contrast to what one would naively expect based on Eqs. 1-3 as these equations predict only an amplitude decrease, while the mode pattern does not change as a function of height.

We observe even stronger pattern changes in the evanescent field of the $m = -1$ harmonic (see Figs. 4e and 4f), for both the experimental result and the FDTD simulation. In both images, the modal pattern is more complex than in Figs. 4a and 4b. In Fig. 4f, several nodes are visible at a height of 200 nm. As the height is increased, only a smooth profile without nodes remains at a height of 1000 nm.

Both the observation of the changes in modal pattern in the images in Figs. 4 as well as the non-single-exponential decay of the $m = -1$ harmonic seen in Fig. 3 deviate from the single exponential decay suggested by a naive interpretation of Eq. 1. The explanation for the deviations from this simple behavior lies in the lateral fields of the harmonics. To build up these complex modal patterns, a range of k_x wavevectors is required. If the magnitude of the k_x wavevectors is comparable to or larger than that of k_y, they need to be taken into account when calculating the decay or the modal pattern of the evanescent field. By substituting $\sqrt{k_x^2 + k_y^2}$ for $k_\parallel$ in Eq. 1 we obtain

$$E(z,t) = E(0,t)\mathrm{e}^{iz\sqrt{\epsilon_{low}\frac{\omega^2}{c^2} - k_x^2 - k_y^2}}. \qquad (4)$$

The k_x wavevectors that make up the lateral patterns are calculated by Fourier transforming the fields and are depicted in Figs. 4c and 4g for the fundamental and $m = -1$ harmonic, respectively. In both figures, the higher k_x values vanish most rapidly as the height increases. Due to the broad range of k_x wavevectors, the decay of even a single Bloch harmonic is not a single exponent, but a multi-exponential decay. We demonstrated the validity of the above argumentation by calculating the field decay and the resulting change in the field pattern as a function of height, using only the experimental data at $z = 10$ nm as a starting point. The result is presented in Figs. 4d

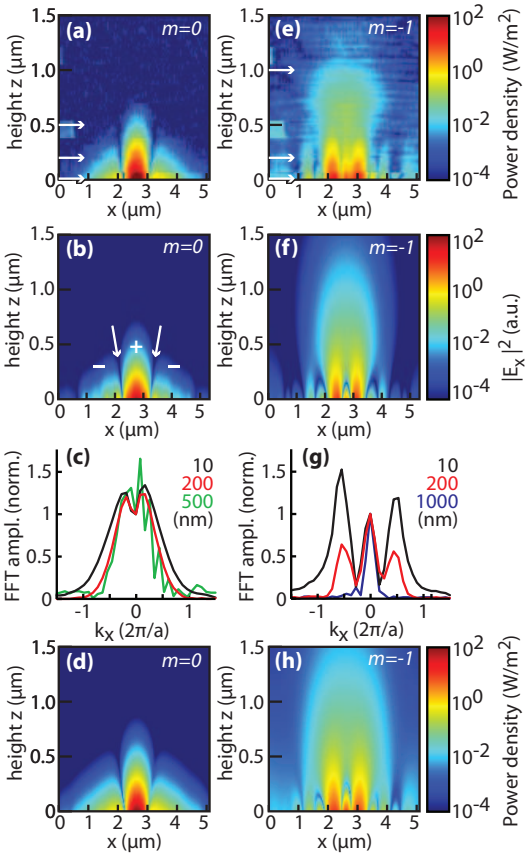

FIG. 4: (a,b) Power density distribution of the fundamental harmonic as a function of height, measured (a) and from FDTD simulation (b). (c) Amplitude of k_x wavevectors obtained via Fourier transformation of the lateral field at heights indicated by the arrows in (a), normalized to the amplitude at $k_x = 0$. (d) Calculated power density distribution by including the decay of k_x wavevectors (see Eq. 4), using the measurements at 10 nm as a starting point. (e-h) Same as (a-d) for the $m = -1$ Bloch harmonic.

and h, which clearly shows excellent agreement with both the full 3D experimental data (Figs. 4a,e) as well as with the 3D FDTD simulation data (Figs. 4b,f).

In conclusion, we have investigated the decay and pattern changes of the evanescent field above a photonic crystal waveguide. Two effects were found that influence the subwavelength pattern and decay of the field. First, the Bloch nature of the propagating mode, which creates an ensemble of wavevectors (k_y), each with their own decay constants, plays an important role. Secondly, the strong confinement of the light in the narrow waveguide plus the intricate lateral mode profile resulting from the neighboring photonic crystal lattice, requires a broad range of wavevectors (k_x) perpendicular to the direction of propagation. The influence of the wavevectors in the x direction results in strong changes of the modal pattern as a function of height above the photonic crystal waveguide, which were found in both near-field experiments and 3D FDTD simulations. The lateral extent of the crystal beside the waveguide, 10 rows in the experiment and 7 rows in the simulations, was sufficient not to influence the the in-plane wavevectors. We expect that if only 4 rows or less would be used, the k_y and k_x wavevectors would differ significantly, which would therefore also affect the subwavelength structure of the evanescent field above the waveguide.

Both the measurements and the simulations show that nanostructured optical materials can have rich evanescent field patterns. This property may be exploited by engineering the geometry such that a specific (subwavelength) evanescent field pattern is obtained, by tuning the k_x wavevectors. This may, for example, be exploited in optical trapping or manipulation of nanoparticles or Bose-Einstein condensates. Promising results have already been demonstrated for tuning of the k_y wavevectors in so-called dispersion engineering in photonic crystal waveguides [19, 20].

The authors acknowledge Femius Koenderink and Silvia Vignolini for enlightening discussions. This work is part of the research program of FOM, which is financially supported by the NWO. Support of the EC-funded project PhOREMOST is gratefully acknowledged. This work is also partially supported by NanoNed, a nanotechnology program of the Dutch Ministry of Economic affairs.

[1] I. Newton, *Opticks* (4th ed., William Innys, London, 1730), Book III, Qu. 29, 346.
[2] M. Cai, O. Painter and K. J. Vahala, Phys. Rev. Lett. **85**, 74 (2000).
[3] D. Rychtarik *et al.*, Phys. Rev. Lett. **92**, 173003 (2004).
[4] T. Aoki, *et al.*, Nature **443**, 671 (2006).
[5] Y. Raichlin, A. Millo and A. Katzir, Phys. Rev. Lett. **93**, 185703 (2004).
[6] R. Merlin, Science **317**, 927 (2007).
[7] L. Kastrup *et al.*, Phys. Rev. Lett. **94**, 178104 (2005).
[8] See for example, C. M. Soukoulis, ed., *Photonic Crystals and Light Localization in the 21st Century*, (Kluwer Academic, Dordrecht, The Netherlands, 2001).
[9] S. Noda *et al.*, Science **289**, 604 (2000).
[10] H. Gersen *et al.*, Phys. Rev. Lett. **94**, 073903 (2005).
[11] Y. A. Vlasov *et al.*, Nature **438**, 65 (2005).
[12] P. St. J. Russell, Appl. Phys. B **39**, 231 (1986).
[13] S. I. Bozhevolnyi *et al.*, Phys. Rev. B **66**, 235204 (2002).
[14] Z. Y. Li and K. M. Ho, Phys. Rev. Lett. **92**, 063904 (2004).
[15] M. L. M. Balistreri *et al.*, Science **294**, 1080 (2001).
[16] H. Gersen *et al.*, Phys. Rev. Lett. **94**, 123901 (2005).
[17] 3D FDTD simulations were performed using a unit cell of $23 \times 267 \times 210$ pixels ($x \times y \times z$), corresponding to $1 \times 11.6 \times 9.1$ lattice periods, with absorbing boundaries conditions for y and z and periodic boundaries for x.

[18] I. P. Radko, S. I. Bozhevolnyi and N. Gregersen, Appl. Opt. **45**, 4054 (2006).
[19] L. H. Frandsen *et al.*, Opt. Express **14**, 9444 (2006).
[20] M. D. Settle *et al.*, Opt. Express **15**, 219 (2007).

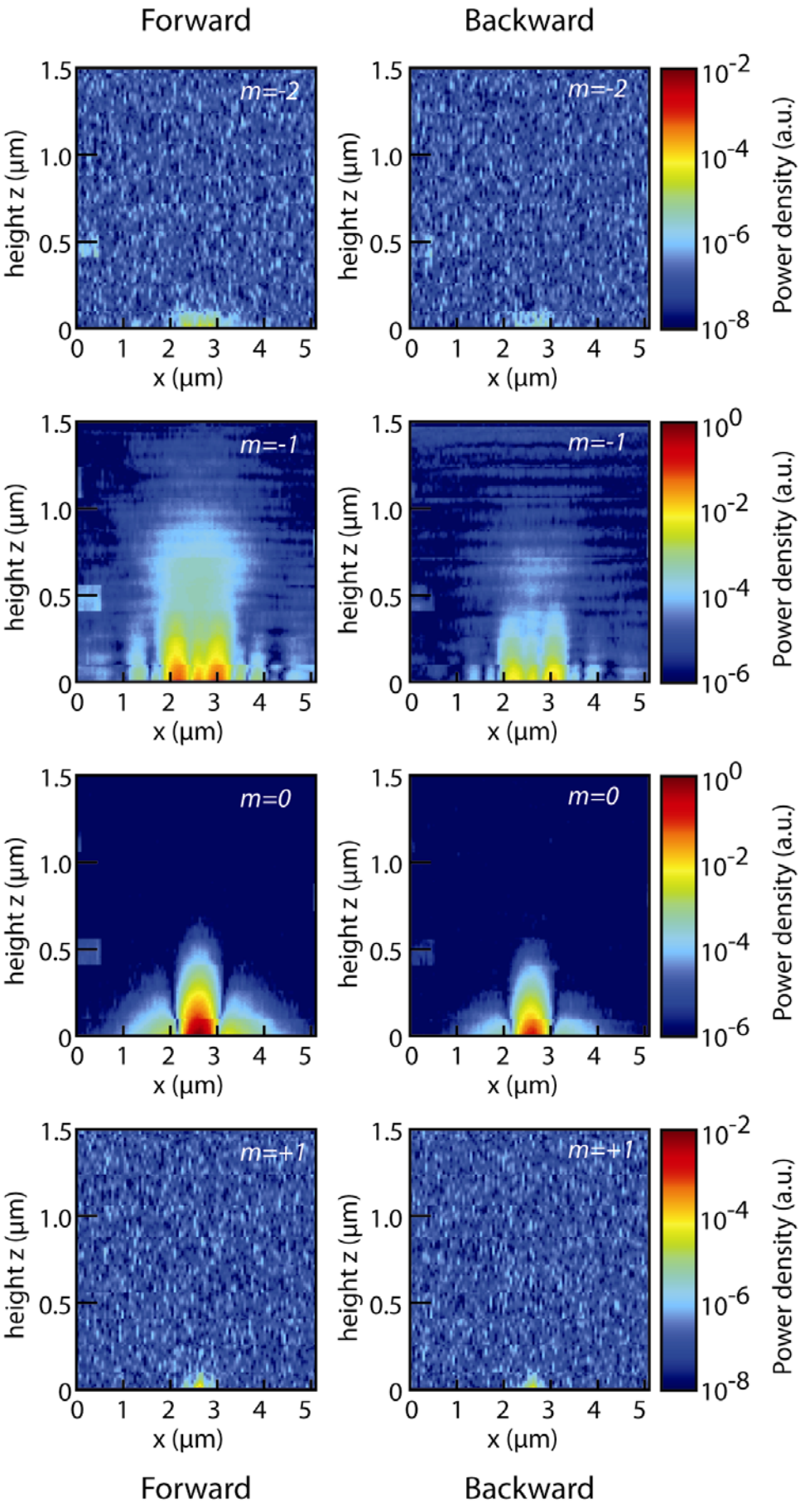
Forward
Backward
m=-2
m=-1
m=0
m=+1
height z (μm)
x (μm)
Power density (a.u.)
0
0.5
1.0
1.5
0 1 2 3 4 5
10-2
10-4
10-6
10-8
100